GeoVirtual 2020 September 14-16
Resilience and Innovation

THE EFFECT OF MECHANICAL LOADING AND CARBONATION ON THE PHYSICAL PROPERTIES OF SOLIDIFIED SAND

Ghassan Aburaas, Jean-Sébastien Dubé & François Duhaime
École de technologie supérieure, Montréal, Québec, Canada
Laboratory for Geotechnical and Geoenvironmental Engineering (LG2)

ABSTRACT
Information on the long-term performances of the stabilization/solidification (S/S) technique under real field conditions remains sparse. In this study, a modified triaxial cell was developed to evaluate the physical properties of silica sand solidified with cement. The modified triaxial cell was required to study the influence of loading and carbonation under a confining stress simulating field conditions. The permeability and compressive strength were measured at different stages of four main scenarios involving carbonation only, axial loading only, carbonation first then loading, and loading first then carbonation. The influence of external loading and carbonation on the physical properties of solidified sand is complex. It involves creating new voids (fractures) that increase the permeability, lower the shear strength, and channel the water flow. It also involves calcite precipitation that fills the pore space with opposite effects on the mechanical and hydrodynamic properties of the solidified sand. Results indicate that the mechanical loading accelerated the damage to the S/S samples and increased their permeability. Deterioration owing to loading decreased in the presence of carbon dioxide. The results of this ongoing study will help to understand the long-term performances of the S/S technique.

RÉSUMÉ
La littérature présente peu d'information sur les performances à long terme de la technique de stabilisation/solidification (S/S) dans des conditions réelles de terrain. Dans cette étude, une cellule triaxiale modifiée a été développée pour évaluer les propriétés physiques du sable de silice solidifié avec du ciment. La cellule triaxiale modifiée a permis d'étudier l'influence du chargement et de la carbonatation sous une contrainte de confinement simulant des conditions de terrain. La perméabilité et la résistance à la compression ont été mesurées à différentes étapes de quatre scénarios principaux impliquant uniquement une carbonatation, uniquement un chargement axial, une carbonatation puis un chargement axial, et un chargement axial puis la carbonatation. L'influence de la charge externe et de la carbonatation sur les propriétés physiques du sable solidifié est complexe. Ces sollicitations créent de nouveaux vides (fractures) qui augmentent la perméabilité, abaissent la résistance au cisaillement et canalisent l'écoulement. Ces sollicitations impliquent également une précipitation de calcite qui remplit l'espace des pores avec des effets opposés sur les propriétés mécaniques et hydrodynamiques du sable solidifié. Les résultats indiquent que la charge mécanique a accéléré les dommages aux échantillons S/S et augmenté leur perméabilité. La détérioration due à la charge diminue en présence de dioxyde de carbone. Les résultats de cette étude permettront de mieux comprendre les performances à long terme de la S/S.

1 INTRODUCTION

The solidification/stabilization technique (S/S) combines waste materials with Portland cement. The resulting material forms a monolith that keeps the waste from contaminating the surrounding water and soil (Richard and Cheyrezy 1995). Cement-based S/S has been comprehensively used for the treatment of contaminated soils for many decades (Al-Tabbaa and Evans 2000). Recently, this process has been considered a promising option in order to provide a solution to what is otherwise a risk to environmental and human health (Al-Tabbaa and Evans 2000). The S/S technique has been shown to be successful when used to immobilize contaminants and to limit the release of some metals (Sanchez et al. 2003). Despite the increased use of S/S, there is a lack of information regarding the long-term stability and performance of this technique (Al-Tabbaa and Evans 2000). Certain environmental conditions can directly influence the performance of S/S in treating waste (e.g., carbonation, elevated temperatures, acidification, freeze/thaw cycles, and mechanical loading).

Fractures and carbonation have a significant impact on the compressive strength and hydraulic performance of the S/S materials. These changes will occur over long periods of time (i.e., perhaps over fifty years or so). Most fractures in S/S materials could also be created and worsened by external stress, hydraulic gradients,

volume expansion, internal stresses, and thermally generated through chemical reactions. It is assumed that cracks typically occur as a result of a higher stress in a specimen (Barenblatt 1959).

However, when stress is distributed over certain areas of a specimen, it creates an energy imbalance and starts to change the shape of voids and induces the coalescence of microcracks in the sample (Barenblatt 1959; Chang and Lee 2004). In general, fracture patterns grow both vertically and horizontally. Additionally, these fractures can intersect or combine to form networks of cracks known as linked cracks (Szeląg 2018). These cracks can be detrimental to the mechanical characteristics of the sample in portions of the sample that are subjected to stress. For example, they are increasing the mobility of contaminants in the short-term and long-term, and minimizing the cohesion of the structure. In particular, the permeability of the samples subjected to mechanical loading was higher than in the original samples (Chang and Lee 2004).

In recent years, considerable interest was also given to the effect of carbonation on S/S. Carbonation is a natural reaction that occurs between carbon dioxide and cementitious materials in the S/S matrix. This phenomenon takes place when carbon dioxide dissolves in the pore solution of the S/S. Following carbonation, CO_2 interacts with calcium hydroxide ($Ca(OH)_2$) to form secondary minerals, mainly calcium carbonate ($CaCO_3$) (Nakarai and Yoshida 2015). The precipitation of calcium carbonate in the pore space will prompt structural changes in the whole monolith or specimen. After exposure to carbonation, pores fill with calcite and this reduces the porosity (Lange et al. 1996).

Other authors have investigated the porosity of S/S monoliths using the adsorption and desorption behavior of water vapor in carbonated and non-carbonated materials (Johannesson and Utgenannt 2001). They concluded that, because calcite in pores has a low solubility, calcite blocks the pores in cementitious materials and change their size distribution. According to Venhuis and Reardon (2001), carbonation leads to an increase in the release of water and a decrease in permeability resulting from a change in pore size distribution. The penetration of carbon dioxide in the pores is usually controlled by static and dynamic processes. For static processes, the water is trapped in pores and prevents CO_2 penetration by diffusion. In dynamic processes, the rate of carbonation is increased by reducing the water content or circulating CO_2 (Bertos et al. 2004).

The penetration depth of carbon dioxide in a cement-soil mixture is usually determined by phenolphthalein spray. There are many other promising techniques used to study carbonation products in pores. For instance, thermogravimetric analysis (TGA), X-ray powder diffraction (XRD), X-ray computed tomography (CT scan), and scanning electron microscopy (SEM) have improved our knowledge regarding calcite formed in pores. Over time, fracturing is inevitable and evolves with the lifetime of the cementitious materials, particularly under natural conditions. Moreover, when the water flows through the sample (pores and fractures), it induces small microcracks to self-repair or to heal (Herbert and Li. 2013). Healing can be divided into three parts: mechanical, physical, and chemical. An example of chemical healing is the formation of calcium carbonate resulting from the reaction between CO_2 dissolved in water and unhydrated cement.

Self-healing is also attributed to continued hydration of cement inside the fractures (Li and Yang 2007). In some circumstances, small fractures heal quickly and completely. This phenomenon depends largely on the width of the fracture (Reinhardt and Jooss 2003). Calcium carbonate is considered to be the principal self-healing material in a soil-cement sample. Although it can close some microcracks and voids, in some other cases, voids might not close because there is an ongoing impact from loading (Taylor. 1997).

As mentioned previously, mechanical damage and carbonation can deteriorate the internal structure in the S/S matrix and create new voids. The objective of this study is to understand the deterioration resulting from the exposure of porous materials (S/S matrix) to mechanical damage and carbonation. To this end, the permeability of S/S samples has been studied under various loading and carbonation conditions.

2 MATERIALS AND EXPERIMENTAL SET-UP

A modified triaxial device was developed to evaluate the permeability for different loading and carbonation scenarios. The development of the triaxial device required 17 months of planning, preparation, and testing. The main goals of the preparation were:

- To determine the appropriate water/cement ratio for the specimens. The ratio was chosen to maximize the percentage of linked voids and to enhance gas penetration.
- To choose the appropriate method of loading. The objective was to generate small cracks. The factors to be considered are confinement pressure, loading stage duration, axial loading rate, and maximum displacement.
- To develop the gas injection protocol. The parameters to be considered are the injection time, gas flow rate, and injection pressure. The protocol was developed to enhance gas penetration through the specimen rather than flow around the specimen.

The permeability coefficient of the material depends on various parameters including the initial porosity distribution, the calcite precipitation and microcracking associated with carbonation, and the effect of loading and unloading. Consequently, the research framework consists of five test protocols. When these test protocols are combined, they can provide a good understanding of the influence of external stress and carbonation on the permeability of S/S materials.

2.1 Material

Cement-based (S/S) specimens were produced by mixing sand and fine gravel particles ranging in size from 0.075 to 6 mm, General Use Portland cement, tap water,

and copper oxide. The grain size distribution of the tested silica sand is shown in Figure 1 (following ASTM C136, ASTM 2006); also, the sand was classified as well-graded sand (SW) based on ASTM D-2487 (ASTM 2011).

2.2 S/S Specimen Preparation

To prepare homogeneous S/S specimens, dry cement, and dry sand and gravel were mixed for five minutes. The tap water and copper oxide were gradually added to the mix together. In order to distribute the components uniformly in the matrix, the material was manually mixed with a trowel for a further 15 minutes.

All specimens were cast in cylindrical molds with dimensions of 50 X 100 mm, and placed in three layers according to ASTM C192 (ASTM 2006). The first two layers were tamped 8 times. The last layer was tamped 9 times.

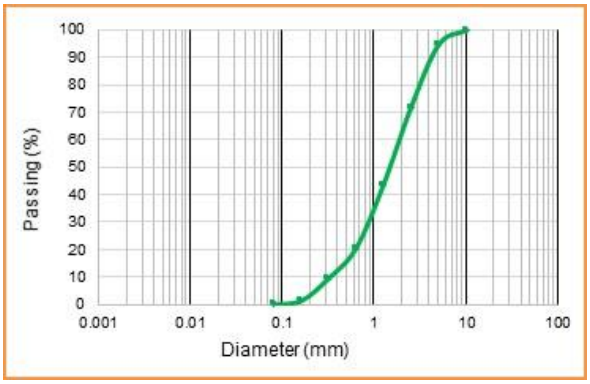

Figure 1. Grain size distribution of silica sand.

To avoid bubbles, each layer was tamped 15 times with a plastic hammer. During the drying process, the specimens were left for 24 hours in the laboratory (at room temperature). After 24 hours, the samples were placed in the humidity room at a relative humidity of 90%. They were demolded after 7 days.

To reduce the reaction with atmospheric CO_2, all S/S specimens were kept in sealed plastic bag and stored in the humidity room to cure for 28 days. All the following experiments were carried out with a modified triaxial cell developed at the soil mechanics laboratory, École de technologie supérieure (ÉTS).

2.3 The Modified Triaxial Cell

A triaxial testing system was used to apply different loading and carbonation scenarios. The triaxial cell allows different confining stresses to be applied to simulate field conditions. The triaxial cell was modified to have the ability to carry out gas flow testing. Moreover, it permits carbon dioxide to be injected in the specimen using high pressure CO_2 gas so that a well-carbonated S/S matrix can be obtained.

The modified triaxial cell is under control for the loading functions, such as the backpressure and the cell pressure. A data acquisition system was used to measure the applied stress, the applied cell pressure, and the pore pressure. Figure 2 shows a cylindrical specimen placed inside the modified triaxial cell.

All tested cylindrical specimens were surrounded by a rubber membrane with a thickness of 0.3 mm to prevent the hydraulic fluid from penetrating the S/S specimen. The membrane was placed in a mold and vacuum was used to remove air between the membrane and the mold. The specimen was then placed inside the mold and the membrane.

The membrane was fixed to the specimen using four O-rings after removing the mold. Two porous stones (discs) were placed at the top and bottom of the specimen. These discs allowed an equal distribution of the pressure on the specimen section.

The modified triaxial cell allowed continuous control of the axial displacement, flow rate of gas (in and out), and flow rate of injected de-aired water (from the top and bottom) during the test. The saturation stage caused all test specimen voids to be filled with water.

Throughout the saturation stage, it was necessary to inject water into the top and base caps of the specimen at the same time. A confining pressure of 50 kPa was applied at the beginning of the saturation stage. The pressure was increased in 50 kPa increments until the cell pressure reached 700 kPa. At the same time, the backpressure and pore pressure were increased to 650 kPa. Two pressure transducers were used to monitor the pressure.

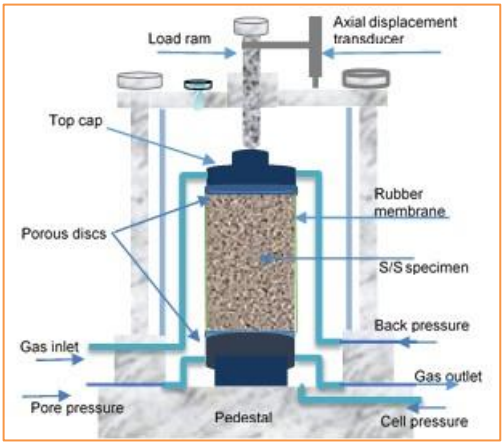

Figure 2. Cross-section of the modified triaxial cell

2.4 Mechanical loading (Initial cracks)

The main objective of the mechanical loading was to create new microcracks in the specimen under a constant confining pressure without the development of wide fractures. A specific procedure of mechanical loading and unloading was followed to this end. The modified triaxial cell enabled the application of loading-unloading cycles on the specimen.

The main two parts of the loading system are a loading frame and a loading control. The loading frame was designed to provide up to 50 kN of axial force.

Mechanical loading was applied through an upward movement of the bottom plate. Deformation was monitored using an axial displacement transducer (LVDT) connected to the top of the specimen (Figure 2). Loading rates were controlled by a computer using software PuTTY.

To ensure drained conditions within the S/S specimen, the axial load was applied at a low rate. The rate of displacement was 0.02 mm per minute, and the maximum displacement required to create fine cracks was 2 mm under drained conditions. The loading-unloading cycles were carried out using the triaxial cell. The duration of the test was 14 hours, i.e., 7 hours of loading and another 7 hours of unloading. The test was finalized with the planned 1.96% deformation.

2.5 Accelerated carbonation

The accelerated carbonation process was carried out using the modified triaxial cell. A strong relationship is observed between the injection pressure of CO_2 and both the diffusion of CO_2 and precipitation of solid phases in the S/S specimen. At low gas pressures, precipitation can close the pores before the carbonation process is finished. Low pressures can decrease the rate of carbonation and reduce the CO_2 diffusion throughout the sample during the injection process (Bertos et al. 2004). Water in the pores necessarily prevents the penetration of CO_2 into the pores of the specimen.

During carbonation, different pressures were applied at the gas inlet and outlet of the specimen (Figure 2). The top tubing was used for gas injection and had a higher pressure. The bottom tubing was used for water removal and had a lower pressure. Water drainage was maintained throughout the carbonation process. This technique allowed the release of water from the sample during its production. Thus, it created a clear pathway that enhanced the penetration of the gas into the specimen before pores closed.

In addition to that, both top and bottom tubes can be used to adjust the pore pressure in the sample. To minimize the effect of calcite precipitation at the beginning of the carbonation process, 100% dry CO_2 gas was injected at a pressure of 710 kPa. During this phase, the pores were still open and the gas penetrated the specimen from top to bottom. The water was drained from the bottom of the sample at 650 kPa. Thus, this procedure increased gas permeability, increased the rate of carbonation, and fully carbonated the specimen.

To allow the full carbonation of the S/S matrix, the cell was kept at a confinement stress of 750 kPa. Over the course of 72 hours, the 100% CO_2 gas was injected directly into the specimen at 710 kPa every 30 minutes for 30 seconds controlled by an electric solenoid valve. Throughout this, the bottom valve was kept open to allow water to drain. During this 72-hour period, the total gas injection time of the specimen was 1.2 hours

2.6 Permeability Test

The permeability tests were carried out according to ASTM D5084 (ASTM 2010), following method C in which variable upstream and downstream water levels were applied. The permeability system consisted of the same modified triaxial cell and a control panel that made it possible to control the applied water pressures. The interpretation of the water flow through the specimen was carried out according to Darcy's law. The hydraulic conductivity is calculated as follows:

$$K = \frac{a_{in} a_{out}\, L}{(a_{in+} a_{out}) A (t_2 - t_1)} \ln \frac{h_1}{h_2} \qquad [1]$$

Where K is the hydraulic conductivity (m/s), a_{in} and a_{out} are the sections of the upstream and downstream burettes; A is the section of the test specimen ($\pi D^2 / 4$); h_1 and h_2 are the head differences between upstream and downstream at time t_1 and t_2, and L is the length of the test specimen.

To facilitate the calculation and interpretation of the test, equation 1 can be transformed into a linear relationship between t and ln(h). The water permeability is then determined from the slope (M) of the linear relationship between ln (h) and t:

$$K = \frac{M\, a_{in} a_{out}\, L}{(a_{in} + a_{out}) A} \qquad [2]$$

2.7 Test Setup

After the test sample was covered in a rubber membrane and it was placed in the triaxial cell. A filter paper was placed at the base and the top of the test sample, and a porous stone. Then, the pressure and water tubes were connected and the sample was placed in the cell, which was filled with de-aired water. The equipment was saturated with de-aired water to remove any remaining air. This was an important step to ensure that no air bubbles remained in the tubes. This can often be done by applying backpressure.

Then, after filling the triaxial cell with de-aired water, a low confining pressure was applied. The ports at the base and the top of the cell were connected to the control panel. At that point, to avoid damage to the sample, a back pressure was applied; this needed to be lower than the confinement pressure by 50 kPa at all times. To saturate the sample the confining pressure and back pressure were applied for a variable periods of time; these were alternated for a total of 24 hours.

The sample saturation stage was verified with the Skempton B coefficient. This coefficient is defined as the ratio of change in pressure of the water in the sample pores to the change in confining pressure. The sample is considered saturated if B ≥ 0.95 or else for incompressible materials if the value of B remains constant with the increase in back pressure (ASTM International D5084, 2003). During the water permeability test, a pressure gradient of 50 kPa was applied.

2.8 Test scenarios

A different specimen was used for each scenario.

a) No Carbonation / No Loading (NC/NL)
After the saturation stage, the specimen was subjected to permeability tests for 10 days.

b) Carbonation (C)
The sample was first subjected to a 24-hour permeability test. Then the sample was injected with gas for 72 hours. Finally, permeability tests were carried out every day for 10 days. The total testing time was 14 days.

c) Mechanical Loading (L)
A 24-hour permeability test was conducted. Then an axial load was applied in 7 hours and removed gradually in 7 hours within the same 24-hour period. Finally, 10 cycles of permeability tests were carried out in 10 days. The total testing time was 13 days.

d) Carbonation Followed by Mechanical Loading (C/L)
A first permeability test was completed after a 24-hour saturation stage. Next, the sample was subjected to carbonation for 72 hours. Then an axial load was applied for 7 hours and removed in 7 hours within the same 24-hour period. Finally, daily permeability tests were carried out for 10 days. The total testing time was 15 days.

e) Mechanical Loading Followed by Carbonation (L/C)
The first permeability test was conducted after a 24-hour saturation stage. Then an axial load was applied in 7 hours and removed in 7 hours within the same 24-hour period. Next, the sample was subjected to carbonation for 72 hours. Finally, the permeability tests were carried out every day for another 10 days. The total testing time was 15 days.

3 RESULTS AND DISCUSSION

A comparison between the K values for the five scenarios shows some significant differences. Table 1 presents the results of the hydraulic conductivity and compressive strength tests for the different scenarios. This table shows the initial K at the first stage of the test and the final K at the end of the test.

Table 1. Results of the hydraulic conductivity and compressive strength tests

Sample number	Compressive strength (MPa)	Initial permeability (m/s)	Final permeability (m/s)
NC/NL	2.18	2.63×10^{-7}	2.16×10^{-7}
C	2.24	7.82×10^{-7}	3.27×10^{-7}
L	2.51	5.20×10^{-7}	2.14×10^{-6}
C/L	2.33	3.76×10^{-7}	4.90×10^{-7}
L/C	2.42	2.10×10^{-7}	4.46×10^{-7}

3.1 No carbonation / No Loading

Figure 3 shows the variation in hydraulic conductivity for the five scenarios as a function of the sequential test number. Different trends were observed for each scenario. The hydraulic conductivity can increase or decrease. The results for each scenario are presented and discussed in the next sections.

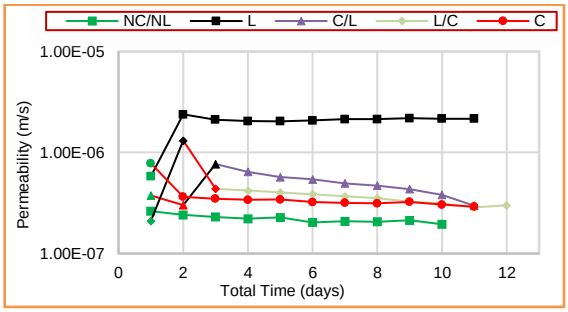

Figure 3. Variation in hydraulic conductivity with time.

The hydraulic conductivity results of the control specimen are given in Figure 4. This scenario does not include accelerated carbonation or mechanical loading. However, after 10 days of maintaining a constant confinement and pore pressure, the hydraulic conductivity results show a gradual reduction of water flow day by day. Each permeability test had a duration of 4.2 hours. Over a period of 10 days, water was injected in the specimen for a total of 42 hours.

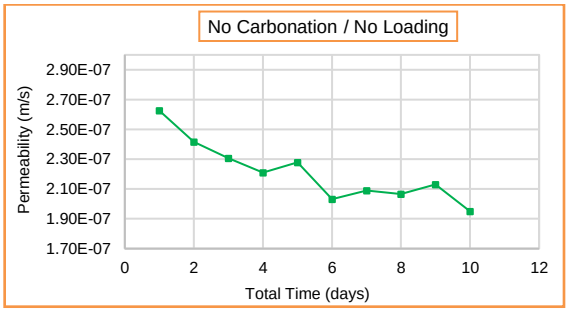

Figure 4. Hydraulic conductivity for the NC/NL scenario.

In general, the hydraulic conductivity was on the order of 2×10^{-7} m/s. The initial K was 2.63×10^{-7} m/s. The K value decreased slightly at the end of the test to reach 1.95×10^{-7} m/s. The decrease in K with time might be caused by the effect of the swelling mechanism (Herbert and Li 2013). According to Yildirim et al. (2015), these mechanisms have the ability to reduce water flow by up to 10%. This finding was confirmed in the present research.

3.2 Carbonation Only

According to Figure 5, a significant decrease in K was observed immediately after carbonation. The K value decreased from 7.82×10^{-7}m/s at the beginning of the test to 3.64×10^{-7}m/s the day after the CO_2 injection. The K value decreased further with time after carbonation. The lowest K value was recorded at the end of the test (2.9×10^{-7} m/s).

The test results indicate that K decreased as a result of calcite precipitation in the pores. Calcite formation (self-healing) took place in linked voids, and induced the pores to close, reducing the number of pores in the specimen.

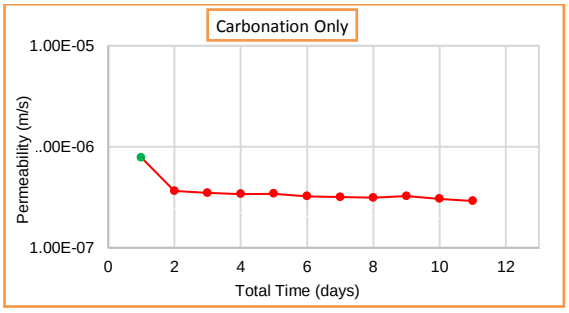

Figure 5. Hydraulic conductivity for the C scenario.

3.3 Loading Only

This scenario created microcracks in the specimen. The specimen presented in Figure 6 shows the initial cracking (damage) after mechanical loading and the K values over time. The presence of microcracks in the specimen increased K and lowered the durability of the specimen.

The K value increased significantly from 5.82×10^{-7} to 2.39×10^{-7} m/s following the loading. It then decreased slightly for the next two days. It reached 2.16×10^{-7} m/s at the end of the test. The value of 2.39×10^{-7} m/s the day after the loading was the highest value recorded during the test. Generally, K decreased only a little over the first five cycles, but this tendency stabilized with time after six cycles of water flow.

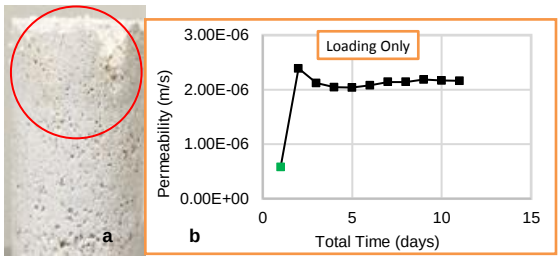

Figure 6. Initial cracking (a) and Hydraulic conductivity (b) for the L scenario.

This scenario can be divided into two main stages. During the first stage, new voids were created by the loading, thus increasing K. The second stage involved a partial healing of these microcracks. It is unclear if this partial healing was caused by clogging from broken particles (Yildırım et al. 2015) or the precipitation of a solid phase. Even with this self-healing, there is still a significant amount of damage in the sample and a higher K at the end of the test.

3.3 Carbonation Followed by Mechanical Loading

The fourth scenario concerned the effect of carbonation and loading on K. The efficiency of the self-healing process depends on both the diffusion of CO_2 and the subsequent growth of calcite in the pores. The influence of accelerated carbonation was different for the C, C/L and L/C scenarios because of the different physical structure of the specimen before and after carbonation. The important physical properties include the presence of linked pores, the existence of microcracks, and the water content in pores.

Figure 7 shows that K initially decreased after carbonation increased after loading and decreased gradually during the permeability tests. The initial K value was 3.76×10^{-7} m/s. After three days of carbonation, the permeability decreased to 3.02×10^{-7} m/s. This corresponds to the effect of the precipitation of calcium carbonate in the pores. Loading was applied in the second phase of the test. As a result the highest value of K was obtained after the loading (7.70×10^{-7} m/s). This increase in K was due to microcracking.

In the last phase, during the permeability test cycles, K decreased gradually until it reached 2.9×10^{-7} m/s. The self-healing process was much more efficient in this case compared to scenario L. The carbonation mechanism (i.e., self-healing) continued and changed the transport properties. The effect of calcite and the water flowing into pores induced the microcracks to heal (Herbert and Li 2013). Consequently, the water permeability coefficient decreased gradually as healing occurred.

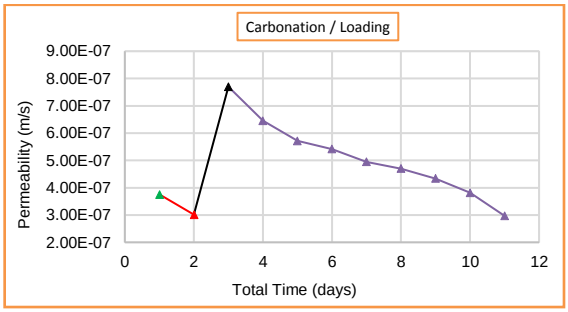

Figure 7. Hydraulic conductivity for the C/L scenario

3.4 Mechanical Loading Followed by Carbonation

The loading and carbonation phases were applied in a different order in this scenario. As we mentioned before, the decrease in water permeability was mainly related to the product of carbonation (healing). The evolution of K during this test protocol is presented in Figure 8.

In the first step, the lowest K value (2.1×10^{-7} m/s) was measured before loading and the occurrence of microcracks. The creation of the first microcracks came after the sample underwent mechanical loading. These microcracks increased K by almost one order of magnitude to reach 1.31×10^{-6} m/s. The highest K value was recorded in this step.

Regardless of the microcracks, the water permeability dramatically decreased after the 72-hour CO_2 injection. The self-healing decreases the water permeability until it reached $4.38x10^{-7}$ m/s. On the other hand, the results show that mechanical loading makes CO_2 diffusion faster and more thorough. This is because loading creates new paths and voids that allow the CO_2 to diffuse. After carbonation, the water penetration into the sample slows due to pores clogging. The K value progressively decreased until reaching $2.87x10^{-7}$ m/s at the end of 10 cycles of water injection.

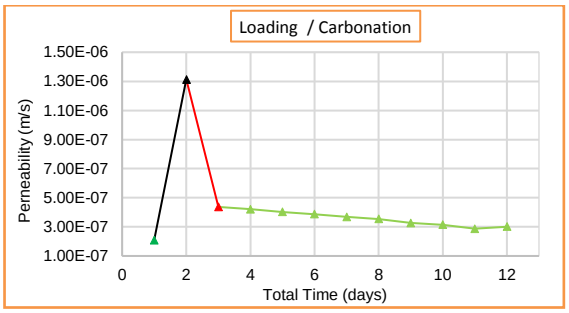

Figure 8. Hydraulic conductivity for the L/C scenario.

4 CONCLUSION

This preliminary study assessed the influence of natural conditions such as mechanical damage and carbonation that affect the hydraulic conductivity of silica sand solidified by cement-based S/S. This methodology can simulate environmental conditions occurring in different test scenarios.

The first test scenario used a control specimen. The K value for this scenario showed a minor decrease. This indicates that the sample heals itself as the water flows through the pores.

The second test scenario involved an accelerated carbonation. The first value of K after carbonation was reduced by 53%. Carbonation created calcium carbonate which closed the pores, resulting in self-healing. By the end of the test, K had gone down by a further 20%.

The third test scenario involved mechanical loading. Due to microcracking, the K increased by slightly more than one order of magnitude. In addition, after 10 days of water injection, because of the phenomenon of self-healing, the water permeability was reduced by 10%. This percentage is similar to the value reported by Yildırım et al. (2015).

The water permeability in the fourth test protocol was evaluated by combining the effects of carbonation and loading. In this test protocol, water permeability was decreased by 20% after the carbonation process. This decrease was due to calcite precipitation in linked voids. After loading the water permeability coefficient was increased by 1.13 orders of magnitude. The next measurement of water permeability was progressively decreased by as much as 21%, i.e., the healing continued until the end of the tests.

In the last test protocol, under mechanical loading conditions, when the microcracks are growing, the results show an increase in water permeability by 1.1 orders of magnitude. These microcracks allow CO_2 penetration. As a result, they diffuse CO_2 through the pores faster than the previous test protocol. Also, during the first cycle of water injection, the permeability was sharply decreased by up to 77%. This reduction of water permeability was gradually slowed down until it was relatively constant during the last four cycles.

Forthcoming work will document further microscale analysis (micro-CT), high-resolution digital imaging, thermal analysis (TGA), chemical analysis, as well as statistical analysis of the previous results.

5 ACKNOWLEDGEMENTS

The authors would like to thank Sébastien Ménard and Maxime St-Jean for their help with the design and construction of the test set-up. The first author would like to thank the Minister of Higher Education in Libya for their support and encouragement.

6 REFERENCES

Al-Tabbaa, A. and Evans, C. 2000. Pilot in Situ Auger Mixing Treatment of a Contaminated Site. Part 3. Time-related performance. *Proceedings of the Institution of Civil Engineers-Geotechnical Engineering*, 143(2), 103-114.

ASTM International. 2006. *Standard practice for making and curing concrete test specimens in the laboratory*. International standard, ASTM C192-07, West Conshohocken (PA).

ASTM International. 2006. *Standard Test Method for Sieve Analysis of Fine and Coarse Aggregates*. International standard, ASTM C136-06, West Conshohocken (PA).

ASTM International. 2011. *Classification of soils for engineering purposes (unified soil classification system)*. International standard, ASTM D2487-06, West Conshohocken (PA).

ASTM International. 2010. *Standard Test Methods for Measurement of Hydraulic Conductivity of Saturated Porous Materials Using a Flexible Wall Permeameter*. International standard, ASTM D5084, West Conshohocken (PA).

Barenblatt, G. I. 1959. The Formation of Equilibrium Cracks During Brittle Fracture. General ideas and hypotheses. Axially-symmetric cracks. *Journal of Applied Mathematics and Mechanics*, 23(3), 622-636.

Bertos, M. F. Simons, S. Hills, C. and Carey, P. 2004. A Review of Accelerated Carbonation Technology in the Treatment of Cement-Based Materials and Sequestration of CO_2. *Journal of hazardous materials*, 112(3), 193-205.

Chang, S.-H. and Lee, C. 2004. Estimation of Cracking and Damage Mechanisms in Rock Under Triaxial Compression by Moment Tensor Analysis of Acoustic Emission. *International Journal of Rock Mechanics and Mining Sciences*, 41(7), 1069-1086.

Herbert, E. N. and Li, V. C. 2013. Self-Healing of Microcracks in Engineered Cementitious Composites (ECC) Under a Natural Environment. *Materials*, 6(7), 2831-2845.

Johannesson, B. and Utgenannt, P. 2001. Microstructural Changes Caused by Carbonation of Cement Mortar. *Cement and Concrete Research*, 31(6), 925-931.

Lange, L. Hills, C. and Poole, A. 1996. The Effect of Accelerated Carbonation on the Properties of Cement-Solidified Waste Forms. *Waste management*, 16(8), 757-763.

Nakarai, K. and Yoshida, T. 2015. Effect of Carbonation on Strength Development of Cement-Treated Toyoura Silica Sand. *Soils and Foundations*, 55(4), 857-865.

Reinhardt, H.-W. and Jooss, M. 2003. Permeability and Self-Healing of Cracked Concrete as a Function of Temperature and Crack Width. *Cement and Concrete Research*, 33(7), 981-985.

Richard, P. and Cheyrezy, M. 1995. Composition of Reactive Powder Concretes. *Cement and Concrete Research*, 25(7), 1501-1511.

Sanchez, F. Garrabrants, A. Vandecasteele, C. Moszkowicz, P. and Kosson, D. 2003. Environmental Assessment of Waste Matrices Contaminated With Arsenic. *Journal of hazardous materials*, 96(2-3), 229-257.

Szeląg, M. 2018. Development of Cracking Patterns in Modified Cement Matrix with Microsilica. *Materials*, 11(10), 1928.

Taylor, H. F. 1997. *Cement Chemistry* (Vol. 2): Thomas Telford London.

Venhuis, M. A. and Reardon, E. J. 2001. Vacuum Method for Carbonation of Cementitious Wasteforms. *Environmental Science and Technology*, 35(20), 4120-4125.

Yildırım, G. Keskin, Ö. K. Keskin, S. B. Şahmaran, M. and Lachemi, M. 2015. A Review of Intrinsic Self-Healing Capability of Engineered Cementitious Composites: Recovery of transport and mechanical properties. *Construction and Building Materials*, 101, 10-21.

Li, V. C. and Yang, E. H. 2007. Self Healing in Concrete Materials. *In Self Healing Materials* (pp. 161-193). Springer, Dordrecht.